Cryodeposit Thin Film Detection Techniques in a High-Vacuum Environment

A Thesis Presented for the
Master of Science
Degree
The University of Tennessee, Knoxville

Sabrina Hope Hurlock
May 2018

ACKNOWLEDGEMENTS

The Author wishes to thank everyone involved in helping with this thesis. First and foremost, thank you to my advisor, Dr. Trevor Moeller, for all of your support, guidance, and patience throughout this process and for giving me the opportunity to work on a project that pushed me and allowed me to grow. Thank you to my committee members, Dr. Monty Smith and Dr. Frank Collins, for your guidance and technical expertise: I truly appreciate all that I have learned from you over the years. Thank you to Doug Warnberg and Joel Davenport for your continued guidance in the lab: without the two of you I would have been truly lost. Thank you to my friends and family for your continued support, encouragement, and for being my inspiration throughout this experience. Thank you to the team at Physical Sciences, Inc., and US Air Force who supported this work. This work was supported by Physical Sciences, Inc. and the US Air Force under contract number FA9550-13-C-0027. This document has been approved for public release under AEDC PA Number AEDC2017-378.

ABSTRACT

It has been well documented that the principal source of contamination for optics in cryogenic systems is water. Prior studies have been successfully performed to explore methods to detect and accurately measure ice growth on optical surfaces. A new setup to detect cryodeposit thin films in high vacuum environments is under development and has been tested at the University of Tennessee Space Institute's (UTSI) Center for Laser Applications (CLA). This setup uses a multiple-beam laser interferometer that is incident the mirror surface at 45 degrees to the normal surface. Water vapor was introduced to the vacuum system via 3-angstrom zeolite molecular sieves, thus allowing ice growth to take place on both a quartz-crystal microbalance (QCM) and a gold-plated first surface mirror. Three experimental runs involving ice-accumulation on the mirror and QCM were performed. Each experimental run lasted for a minimum of two hours in order to allow a significant amount of ice to form on the test surfaces. Using data from both the QCM and multi-beam interferometer, we were able to effectively and non-invasively measure the accumulated cryogenic ice layer thickness. During the final two-hour and thirty-two-minute run on November 26th, 2013, we obtained ice thickness values of 3.25 micrometers and 2.88 micrometers with the interferometer and QCM, respectively. The thickness values measured by the QCM and interferometer were within 12.2% of each other.

TABLE OF CONTENTS

LIST OF TABLES

LIST OF FIGURES

CHAPTER ONE
INTRODUCTION AND BACKGROUND

1.1 Overview and Purpose

Water condensation and ice formation on surfaces in cryo-environments is a serious problem for any type of sensitive instrumentation. This water deposition can cause a whole host of problems from electronic shorts and reduced instrument sensitivity to complete system failure. Research conducted at the University of Tennessee Space Institute (UTSI) is geared toward developing a mitigation technique to reduce, if not all together eliminate, the effects of water deposition. The purpose of this project was a feasibility study to demonstrate that the vacuum chamber-interferometer-QCM system at UTSI was capable of measuring the thickness of the cryodeposit layer on a first-surface gold-plated mirror and QCM.

Building off of the work performed by James Rogers in his master's thesis [13], a similar technique of water deposition on surfaces in a cryocooled vacuum chamber was utilized. Housing a zeolite molecular sieve sample in a small, external, individually pumped-down sample chamber, water vapor was release from the sample and into the main vacuum chamber via an effusion cell. Due to the extremely cold temperatures inside the chamber, the water vapor quickly condensed to form a very thin ice layer on both the quartz-crystal microbalance (QCM) and gold-plated mirror surfaces. The cryodeposit thickness was then determined by both analyzing the QCM data and data obtained by the multi-beam interferometer.

Data from a residual gas analyzer (RGA) was used to determine if there were any contaminant gases in the chamber that would negatively impact the outcome of the ice thickness

monitor results. Fortunately, our system had only trace amounts of other gases that were most likely due to small amounts of air entering the system via a virtual leak in the valve isolating the exterior sample chamber from the main vacuum chamber.

1.2 Cryodeposit Thin Films in Space and Space-Like Environments

As of the writing of this this thesis, there are well over one thousand satellites in orbit around the Earth [7]. Billions of dollars and man-hours have gone into the design, building, launch, and maintenance of these satellites.

Working with optical components in space and space-like environments comes with its own set of hurdles to overcome. Many of the components used in laboratory experiments or space satellites are exposed to temperatures as low as 4 Kelvin (-269°C or -452°F) and pressures in the range of 10^{-9} - 10^{-6} Torr [4].

One of the side effects of operating machinery in such extreme environments is the deposition of material onto the optical components. It is known that in space and space-simulated vacuum environments, optical components can still be exposed to contamination by gases and molecules, which can result in a thin layer of material forming on the optical surfaces. Once this thin film has accumulated on the optical surface, a multitude of problems can occur, ranging from inaccurate measurements to complete component failure.

The sources for thin film contamination are varied depending upon the environment, and the methods for eliminating the contaminants are equally complicated. On Earth, the likelihood of contamination is quite high. Even though we can simulate a space-like environment, it is still contained in a man-made structure that has been exposed to the atmosphere. The materials used

to construct vacuum chambers are rough and are susceptible to absorption of gases and other molecules, such as water. When a vacuum chamber is pumped down and cooled to simulate the environment in space, these particles are released from the rough surface material and can accumulate on the cold surface of the components being tested (e.g., ice accumulating on an optical surface, such as a lens or mirror).

In space, thin film contamination can come from naturally occurring water particles found in space [19, 20, 22], outgassing of satellite components once exposed to ultra-low pressures, or by the combustion of spacecraft propellants [8]. This is a much more difficult situation to rectify due to our inability to easily reach the equipment.

1.3 Thin Film Detection: Interferometer

In order to measure the ice thickness and accumulation rates on the gold mirror, the physics governing multi-beam interference in thin films were applied. Any time light impacts the surface of a thin film, three processes occur: depending on what the thin film is made of, some of the light is reflected, some is absorbed by the material, and the rest is transmitted. A diagram representing the reflection and transmission of light though a thin film on a gold surface is shown in Figure 1.1 [21]. In this particular instance, the single beam of light that was emitted began to interfere with itself, when it struck and reflected through the thin layer of ice. As can be seen in Figure 1.1, as the light reflected in the thin film, a component of the light continued to reflect off of the upper and lower boundaries of the ice film, while others continued to be transmitted. It is important to note that both the reflected and transmitted rays are parallel to each other and also

have different phases. The parallel reflected and transmitted rays can then be focused by a lens and onto a photodiode, where the interference pattern can be analyzed.

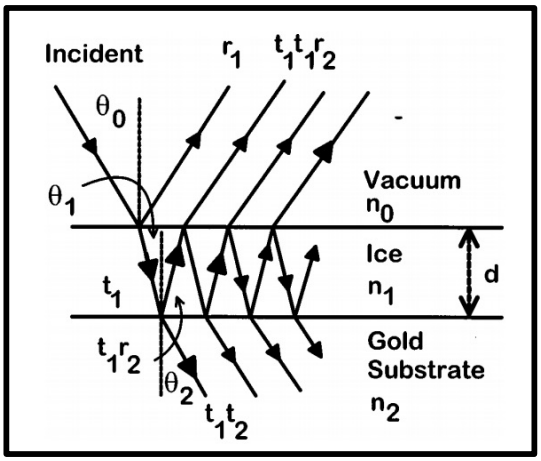

Figure 1.1. Reflection of a Thin Film.

Using the Fresnel equations given below, we can calculate the field amplitude coefficients of the reflected (*r*) and transmitted (*t*) light,

$$r_{1,s} = \frac{n_0 * \cos\theta_0 - n_1 * \cos\theta_1}{n_0 * \cos\theta_0 + n_1 * \cos\theta_1} \quad (1)$$

$$t_{1,s} = \frac{2 * n_0 * \cos\theta_0}{n_0 * \cos\theta_0 + n_1 * \cos\theta_1} \quad (2)$$

where n_1 is the index of refraction for the ice film, n_0 is the index of refraction for the vacuum, r_1 and r_2 are the amplitude ratios of the reflected waves, and t_1 *and* t_2 are the amplitude ratios of the transmitted waves, as shown schematically in Figure 1.1 [21]. Note that these equations apply to light that has been perpendicularly polarized to the plane of incidence: this will be discussed in both Section 2.4 and Section 4.1.

Because the incident light came into contact with and passed through the thin ice film, we also had to take into consideration the phase change of the light as it transmitted through the ice. The derivation for this process was shown in detail in Westley, et.al. 1998, but in summary, in

order to find the magnitude of the reflected light, R, we had to add together all of the reflected rays and apply conservation of energy in order to obtain the expression

$$\boldsymbol{R} = \left|\frac{r_1 + r_2 e^{-2i\delta_1}}{1 + r_1 r_2 e^{-2i\delta_1}}\right| \quad (3)$$

where we are able to get a value for the reflected light intensity ratio $|R|^2$ [6, 21].

1.4 Thin Film Detection: Quartz-Crystal Microbalance (QCM)

A quartz-crystal microbalance (QCM) was used in conjunction with the cryo-cooled gold-plated mirror to substantiate the ice thickness data obtained from the interferometer. A QCM operates by comparing the natural resonant frequency of the crystal to the frequency measured after any mass has accumulated on the surface [10, 11, 15]. By comparing the resonant frequency to the new frequency after mass accumulation do to a thin film, the total mass of the thin film was able to be determined.

In a crystal, the natural frequency is given by

$$\boldsymbol{f_0} = \frac{\sqrt{\mu_q/\rho_q}}{2t} \quad (4)$$

where μ_q is the shear modulus of quartz, ρ_q is the density of quartz, and t is the crystal thickness [11].

We must take into consideration the shift in frequency that occurs when a thin film begins to deposit on the QCM surface [11]. The equation for the change in frequency is given by

$$\Delta \boldsymbol{f} = \boldsymbol{C_f \Delta m} \quad (5)$$

where, Δm is the change in mass and C_f the sensitivity factor and is given by

$$C_f = \frac{2nf_0^2}{\sqrt{\rho_q \mu_q}} \quad (6)$$

where n is the driving harmonic for the crystal, f_0 is the natural frequency of the crystal, μ_q is the shear modulus of quartz, and ρ_q is the density of quartz [12, 14].

As described in Moeller et.al. 2012, instead of using Equation 6 above, the Z-match technique was utilized to determine the mass. In order to find the mass per unit area, the following equation was used:

$$Z = \sqrt{\frac{\rho_q G_q}{\rho_f G_f}} \quad (7)$$

where ρ_f is the density of ice, G_f is the shear modulus of ice, ρ_q is the density of quartz, and G_f is the shear modulus of quartz [11].

For this series of experiments, we used the Inficon QPod with an Inficon 6 MHz gold-plated crystal in a Maxtek housing. Additionally, we used the following values to determine the ice accumulation mass values:

$$\rho_f = 0.94 \text{ g/cm}^3$$

$$G_f = 3.6 \times 10^{10} \text{ dyne/cm}^2$$

$$\rho_q = 2.648 \text{ g/cm}^3$$

$$G_q = 2.947 \times 10^{11} \text{ dyne/cm}^2.$$

As will be discussed Section 4.2, the program QCM_Anal [18] calculated the ice thickness by using the equation

$$x(t) = \sqrt{\frac{\mu_{quartz}\rho_{quartz}}{2f_0\rho_{ice}}}[f_0 - f(t)] \quad (8)$$

where t is time (not thickness), f_0 is the unloaded quartz crystal frequency of oscillation, and $f(t)$ is the resonant frequency at a particular time t.

CHAPTER TWO
INSTRUMENTATION AND TEST SETUP

2.1 The UTSI Vacuum Chamber

In August 2010, the Solar Absorptance Measurements (SAM) vacuum chamber was donated to the University of Tennessee Space Institute (UTSI) by AEDC (Arnold Engineering and Development Complex). According to a report by W. T. Bertrand, this chamber was originally "developed to measure the change in integrated solar absorptance of aluminum coated mirrors by condensed outgassing contaminants irradiated by a solar simulator under vacuum" [2]. The SAM chamber now resides in the vacuum chamber area of the Center for Laser Applications (CLA) at UTSI.

The SAM chamber utilizes an Osaka Vacuum model TG220FRAB turbo molecular pump that is capable of 210 L/s of N_2 volume flow rate. After characterization of the chamber, the lowest recorded pressure was 6.03×10^{-9} Torr: the chamber characterization is summarized in Table 2.1. It is cooled by a Sumitomo CH-210 cold head assembly cryocooler (coldfinger) driven by a Sumitomo F70L helium compressor module. The first stage is capable of providing a 120 Watt cooling capacity at 77 K, while the second stage is capable of a 7.0 Watt cooling capacity at 20 K. The chamber pressure is monitored by Kurt J. Lesker convection and ion gauges (details on these gauges will be presented later). A top-view schematic of the chamber and interferometer setup is shown in Figure 2.1, while a labeled photograph is shown in Figure 2.2.

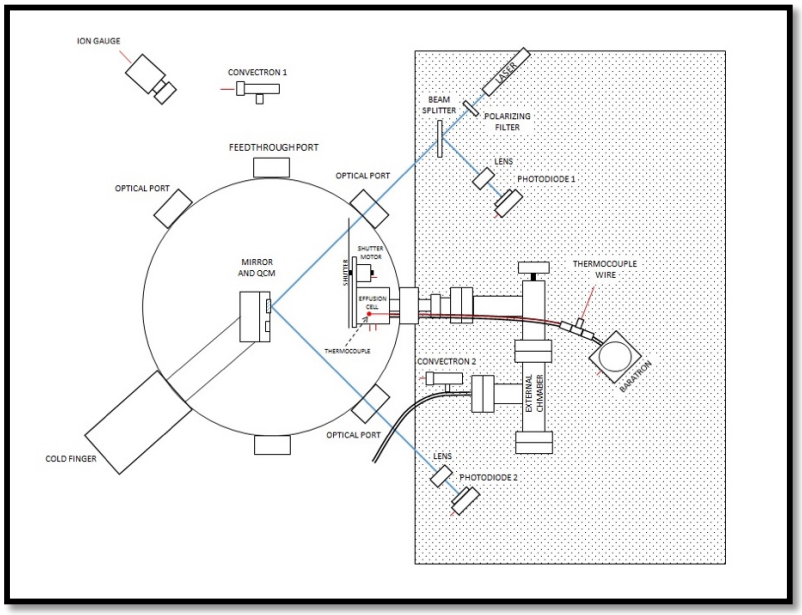

Figure 2.1. Schematic of the Chamber and Interferometer Setup at UTSI.

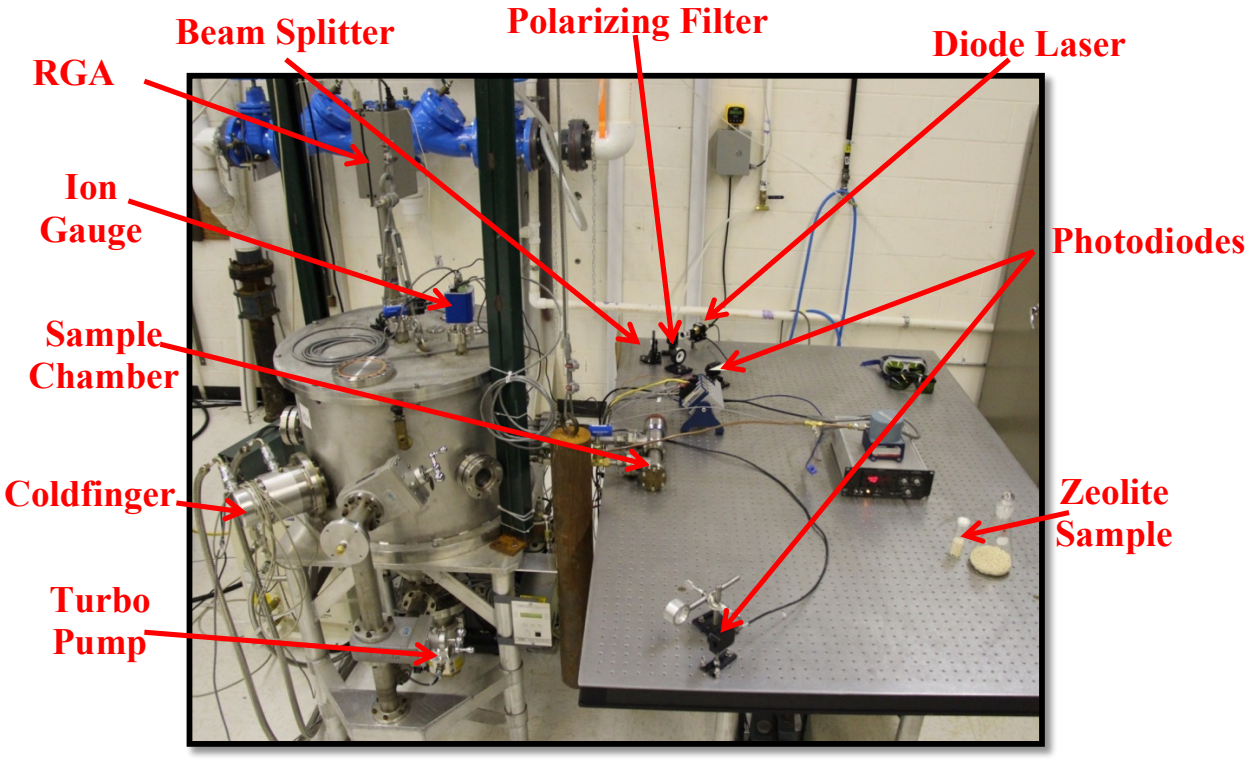

Figure 2.2. Photograph of the Chamber and Thickness Monitor Setup at UTSI.

Table 2.1. UTSI Vacuum Chamber Characteristics.

External Characteristics	
Height:	45.4 cm
Diameter:	60.5 cm
Volume:	130.5 L
Internal Characteristics	
Height:	40.2 cm
Diameter:	52.7 cm
Volume:	87.7 L
Lowest Recorded Pressure (prior to cooling)	5.40×10^{-6} Torr
Lowest Recorded Pressure (after cooling)	6.03×10^{-9} Torr
Lowest Temperature	29.28 Kelvin

2.2 Test Setup and Components

The test articles housed in the chamber interior required for depositing and monitoring water-ice growth were an effusion cell, a gold-plated first surface mirror, and a quartz-crystal microbalance (QCM) (see Figures 2.1 and 2.3). Both the mirror and QCM were encased and attached to a mount (see Figure 2.4), which sat atop an aluminum block that was attached to the arm of the cryocooler and held in place by a C-clamp. Strips of indium were placed on the aluminum block to improve heat conduction between the block and the mount. Temperature changes for the mount were monitored by a thermocouple (see Figure 2.4) and a CLTS (cyrogenic linear temperature sensor) temperature sensor affixed to the back of the mirror housing unit (see Figure 2.5). The front of the mirror/QCM mount sat parallel to the face of the effusion cell (see Figure 2.5) to ensure water vapor was evenly distributed on both the QCM and mirror surfaces.

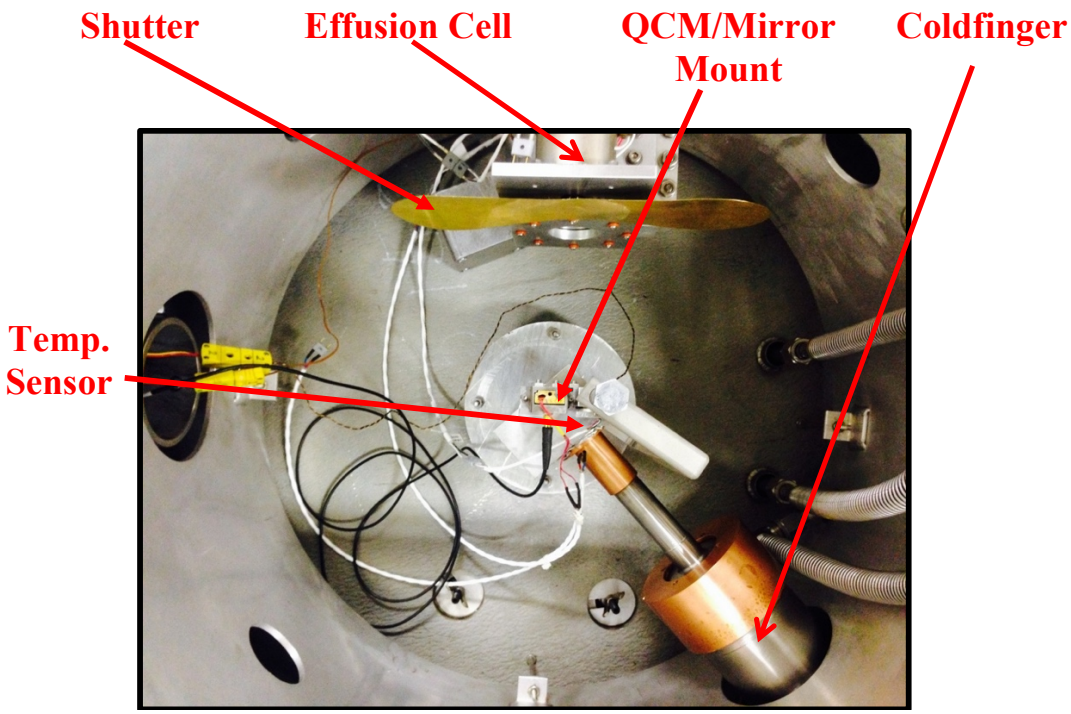

Figure 2.3. Aerial View of UTSI Vacuum Chamber Interior.

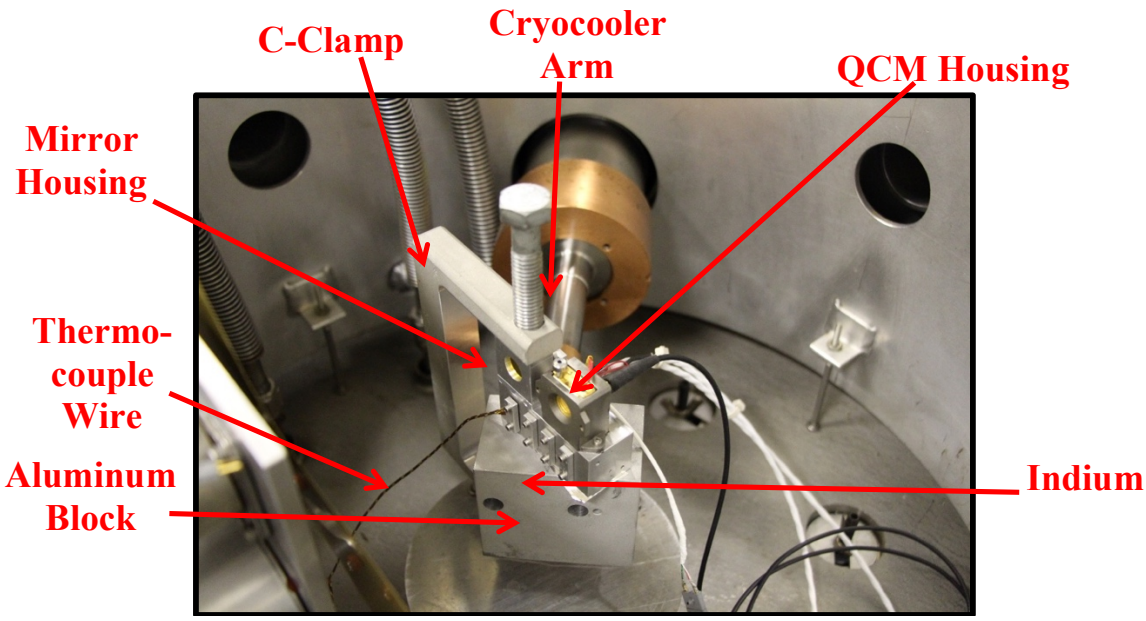

Figure 2.4. QCM and Mirror Mount Setup.

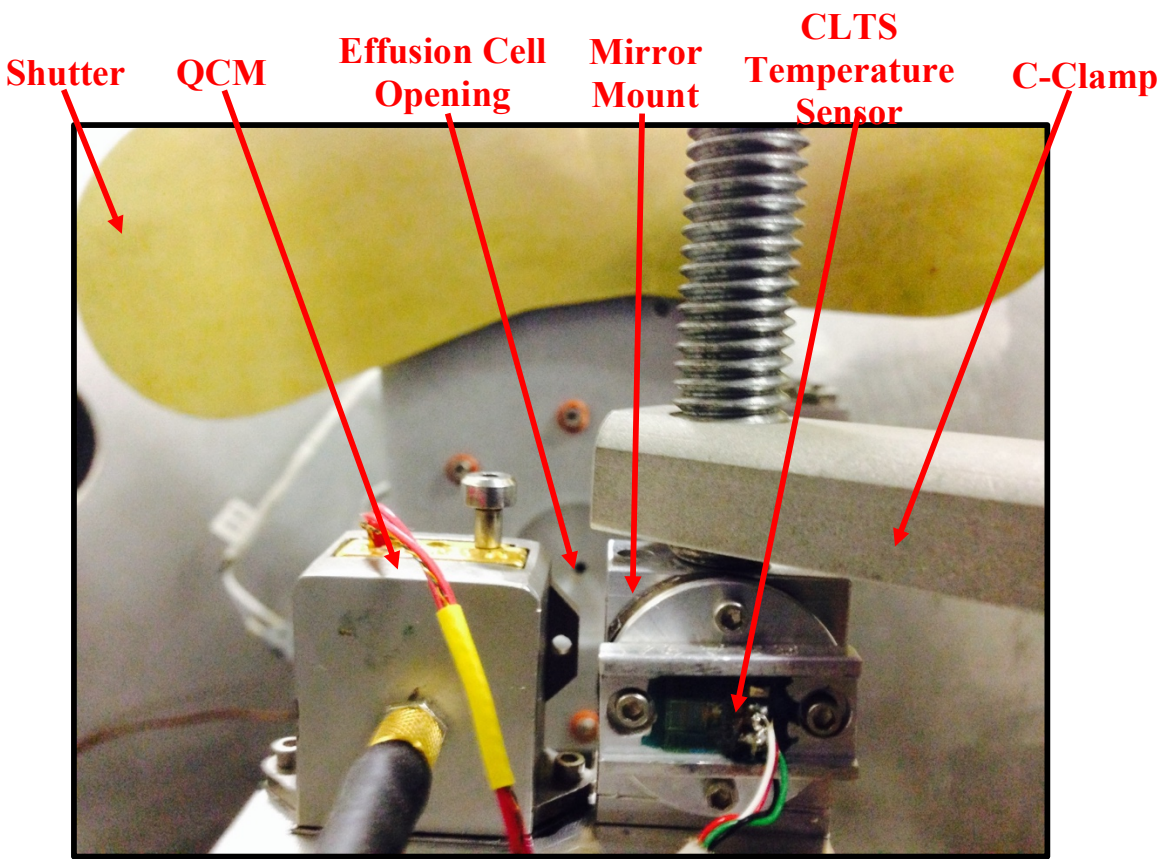

Figure 2.5. Close-Up Interior View of the QCM, Mirror, and Effusion Cell Setup.

2.3 Zeolite Molecular Sieves

Zeolite molecular sieves were used to introduce water to the vacuum chamber. These sieves are used in various applications as a way of drying, purifying, and separating gases and liquids [1]. Zeolite is, in essence, a 'molecular sifter' in that the sieve has the ability to separate molecules based upon their size, shape, and polarity by way of a "network of crystalline micropores that form molecular-sized voids and channels inside their crystalline structure," [13, 23].

There are two common types of zeolites sieves, Linde Type A and X, the properties of which are summarized in Table 1.1 [1]. For the purposes of this study, we only considered the Linde Type A, hereafter referred to as the LTA, sieve. The LTA naming convention is based upon the pore diameter, in Angstroms: a sieve with a 3 Angstrom pore diameter is classified as Type 3A, a sieve with a 4 Angstrom pore diameter is a Type 4A, etc.

Table 2.2. Zeolite Molecular Sieve Properties [1].

Type	**Nominal Pore Diameter** (Angstroms)	**Common Form**	**Bulk Density** lb/cu-ft (gm/cc)	**Heat of Adsorption** (max) btu/lb H_20 (kcal/kg H_2O)	**Equilibrium H_2O Capacity** wt-%	**Molecules Absorbed**
3A	3	Powder 1/16-inch Pellets 1/8-inch Pellets 8x12 Beads 4x8 Beads	35 (0.56) 40 (0.64) 40 (0.64) 44 (0.71) 44 (0.71)	1800 (1000)	26 21 21 21 21	Molecules with an effective diameter <3 angstroms including H_2O and NH_3
4A	4	Powder 1/16-inch Pellets 1/8-inch Pellets 8x12 Beads 4x8 Beads 14x30 Mesh	32 (0.51) 44 (0.71) 44 (0.71) 44 (0.71) 44 (0.71) 44 (0.71)	1800 (1000)	27 22 22 22 22 22	Molecules with an effective diameter <4 angstroms including H_2S, CO_2, SO_2, C_2H_4, C_2H_6, and C_3H_6
5A	5	Powder 1/16-inch Pellets 1/8-inch Pellets	32 (0.51) 44 (0.71) 44 (0.71) 21	1800 (1000)	26 21.5 21.5	Molecules with an effective diameter <5 angstroms including n-C_4H_9OH, n-C_4H_{10}, C_3H_8 to $C_{22}H_{46}$, R-12
13X	8	Powder 1/16-inch Pellets 1/8-inch Pellets 8x12 Beads 4x8 Beads	27 (0.43) 40 (0.64) 40 (0.64) 40 (0.64) 40 (0.64)	1800 (1000)	30 26 26 26 26	Molecules with an effective diameter <8 angstroms including C_6H_6, C_7H_8

The first question that needed to be considered was this: How do we know which zeolite sieve is the best option for introducing water to our vacuum system, while reducing the amount of non-water contaminants? In order to answer this question, a more detailed understanding of how a zeolite sieve actually works was needed.

In the work of D.W. Breck [3], it was discussed that, while the Type 4A zeolite sieve is known to adsorb H_2O, CO_2, SO_2, H_2S, C_2H_6, and ethanol, the Type 3A zeolite sieve will adsorb only H_2O with trace amounts of NH_3 and possibly a very small amount H_2 [1, 3, 13]. Because a water molecule has an approximate diameter of 2.7 Å, the Type 3A zeolite sieve was selected for use in chamber hydration due to its ability to adsorb water molecules with the lowest possibility of contamination of other types of molecules.

The aperture of a zeolite sieve will allow a molecule, due to its dipole-cation interactions and vibrational motion [13], of a size up to 0.5 angstroms larger than the free diameter of the aperture [1]. The Type A zeolite sieve can be described as spherical, for all intents and purposes, and contains small cavities that are approximately 11 angstroms in diameter and 925 cubic angstroms in volume [1]. As summarized on the University Oil Products website [1] and referring to Figure 1.1:

"The type a molecular sieve has a framework composed of truncated octahedral joined in a cubic array. The result is a central truncated cube-octahedron with an internal cavity, 11 angstroms in diameter (alpha cage). Each central cavity, or alpha cage, is entered through six circular apertures formed by a nearly regular ring of eight oxygen atoms with a free diameter of 4.2 angstroms. The cavities are arranged in a continuous three-dimensional pattern forming a system of unduloid-like channels with a maximum diameter of 11 angstroms and a minimum of 4.2 angstroms. The truncated octahedron encloses a second set of smaller cavities 6.6 angstroms in internal diameter (beta cages). The smaller cavities are connected to the larger cavities via a distorted ring of six oxygen atoms of 2.2 angstroms free diameter." [9]

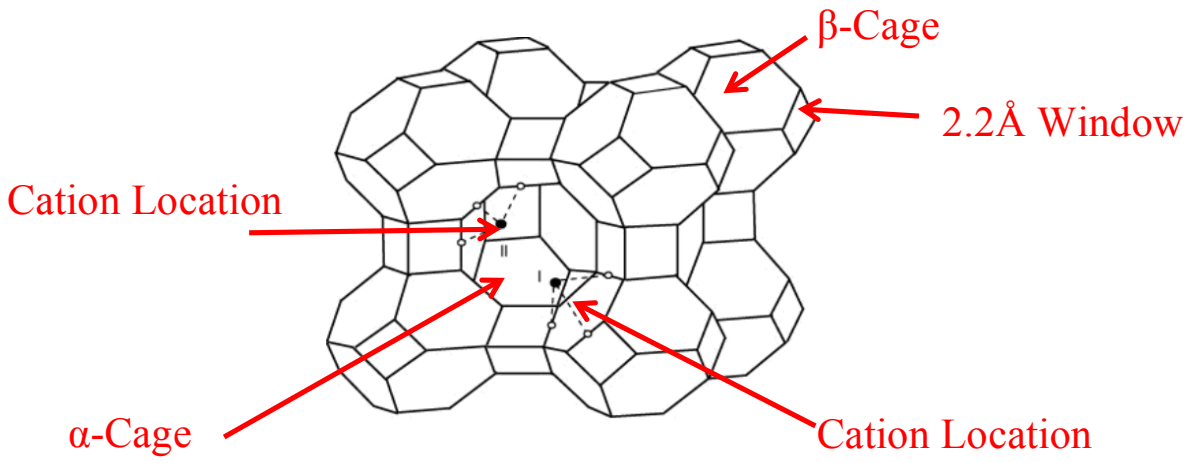

Figure 2.6. Zeolite Molecule [9, 13].

As stated previously, water molecules can enter the zeolite sieve through the windows by means of vibrational motion or dipole-cation interactions [13]. The beta cages, having a 6.6 angstrom diameter, can hold up to eight water molecules, in which they will either hydrogen bond to each other or coordinate with (bond to) oxygen atoms in the framework of the cell, if these are the atoms that are closest to the molecule [9, 13]. The alpha cages, with a free diameter of approximately 11 angstroms, can hold up to twelve water molecules [22] where they will hydrogen bond with each other, coordinate with the framework oxygen atoms, and/or associate with the cations (refer to Figure 1.1) [13].

2.4 Ice Thickness Monitor Setup

External to the chamber and mounted on an "optical breadboard" table are the components of the optical interferometric ice thickness monitor: the laser, photodiodes, and associated beam splitter, lenses, and polarizing filter. In addition, the canister housing the molecular sieve water source (see Figure 2.7) and its associated instrumentation (a baratron

pressure gauge, thermocouple temperature measurements) are positioned on the table (see Figure 2.8). Other instrumentation and operating equipment (e.g., convectrons, ion gauges, coldfinger, and feedthroughs) are shown in Figure 2.2 in their respective locations, while the effusion cell shutter control is shown in Figure 2.9.

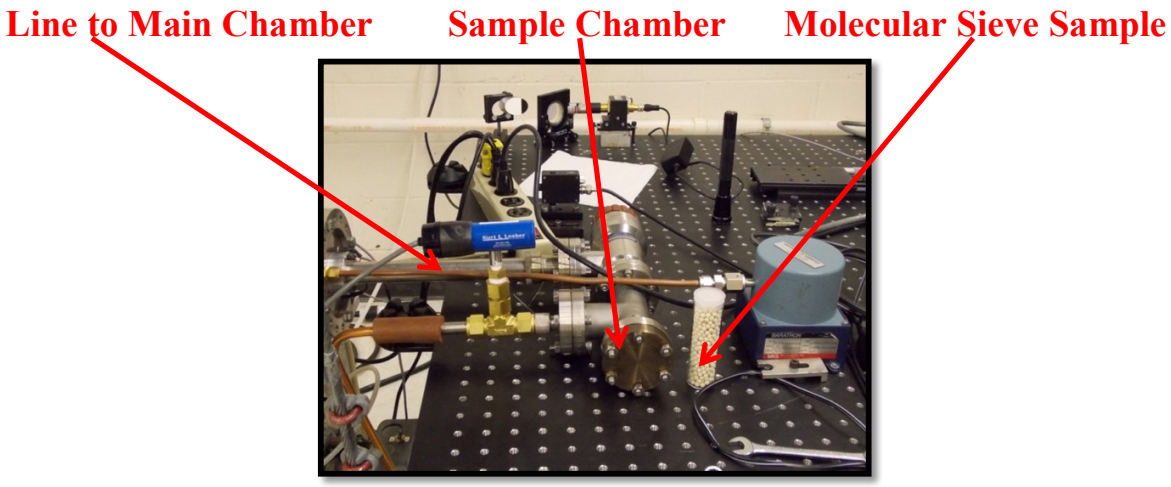

Figure 2.7. Molecular Sieve Sample and Sample Chamber

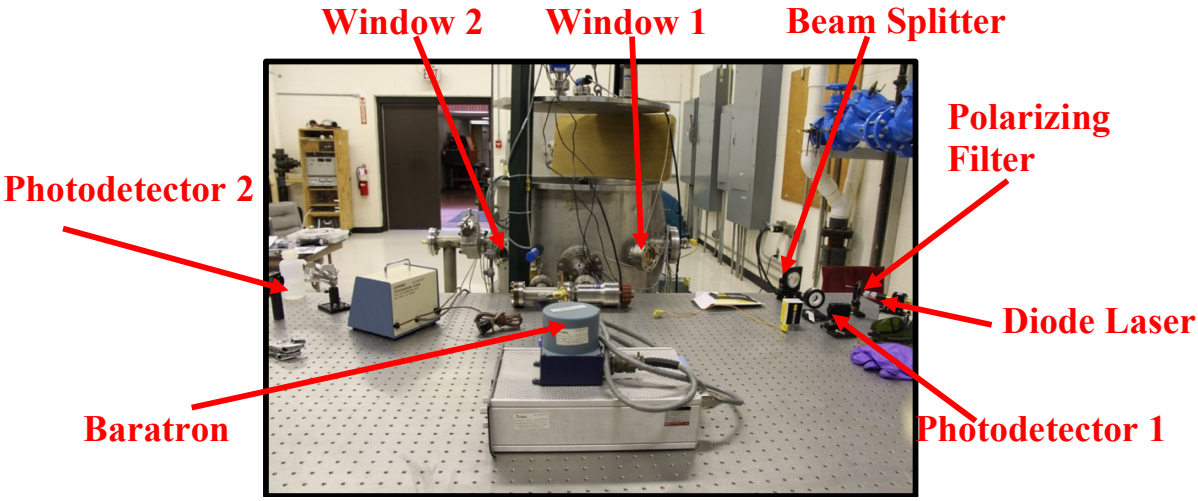

Figure 2.8. Eye-level View of the Optical Setup.

Figure 2.9. Effusion Cell Shutter Control

The layer of ice formed as the water vapor plume condensed is monitored with two different methods: multiple-beam interference resulting from the thin film of ice on a first-surface gold mirror (as described in Section 1.3) and a quartz crystal microbalance (see Section 1.4). The gold-plated mirror, shown in Figure 2.10 (Edmunds Optics Model NT43-404-566), constitutes an optically flat substrate for the ice film.

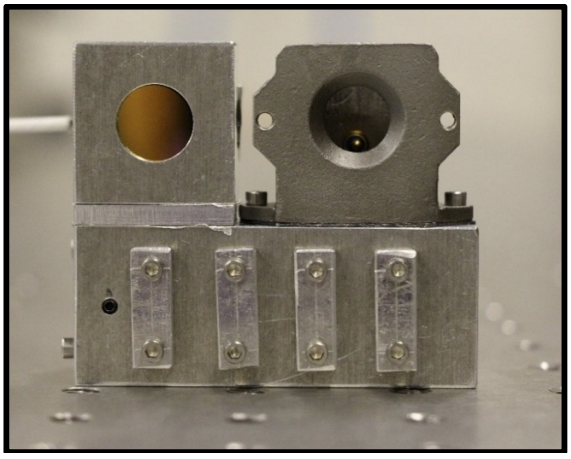

Figure 2.10. Gold-Plated Mirror

Optical data from the incident and reflected laser beams were collected using two ThorLabs silicon-based photodiodes (Thorlabs Model DET10A, 200-1100 nm spectral range) located on the table adjacent to the main vacuum chamber. The first photodetector monitored the light intensity output from the diode laser (Edmunds Optics Model 64-819, 20mW output power, 450 nm wavelength), while the second photodetector measured the intensity of light reflected from the gold-plated mirror (Edmunds Optics Model NT43-404-566) inside the chamber. The ratio of photodiode voltages thus constituted a reflectance of the ice/mirror surface in arbitrary units, which was then digitized and stored for post-test data processing. It is important to note that the polarizing filter shown in Figure 2.8 ensures that the light emitted from the laser is perpendicular to plane of incidence of the gold mirror; this is important because the laser beam was not initially perpendicular to the mirror.

An eye-level view of the optical components is depicted in Figure 2.8. As shown in the figure, the beam from the diode laser passes through Window 1 on the right in the photograph, into the vacuum chamber, reflects off the surface of the mirror accumulating a layer of ice, and then exits the chamber through Window 2 on the left in the photograph.

CHAPTER THREE
EXPERIMENTAL PROCEDURE AND BASELINE TEST

3.1 Test Procedure

The experimental procedure for a typical test is outlined as follows:

After the SAM chamber was initially pumped down with the Osaka turbo pump (see Figure 3.1) and reached the minimum target pressure of 10^{-6} Torr, the coldfinger (see Figure 2.3 in test setup section) was activated to cool the chamber to the required 20-30 Kelvin. Once the ideal pressure and temperature had been reached, 10^{-6} Torr and 20-30K, respectively, data were recorded using the following software: LabView for the temperature, pressure, and optical light intensity measurements (see Figure 3.2); manufacturer-supplied RGA software for partial pressure measurements of the gases present in the chamber, and manufacturer-supplied software for the QCM.

Figure 3.1. Osaka Turbo Pump

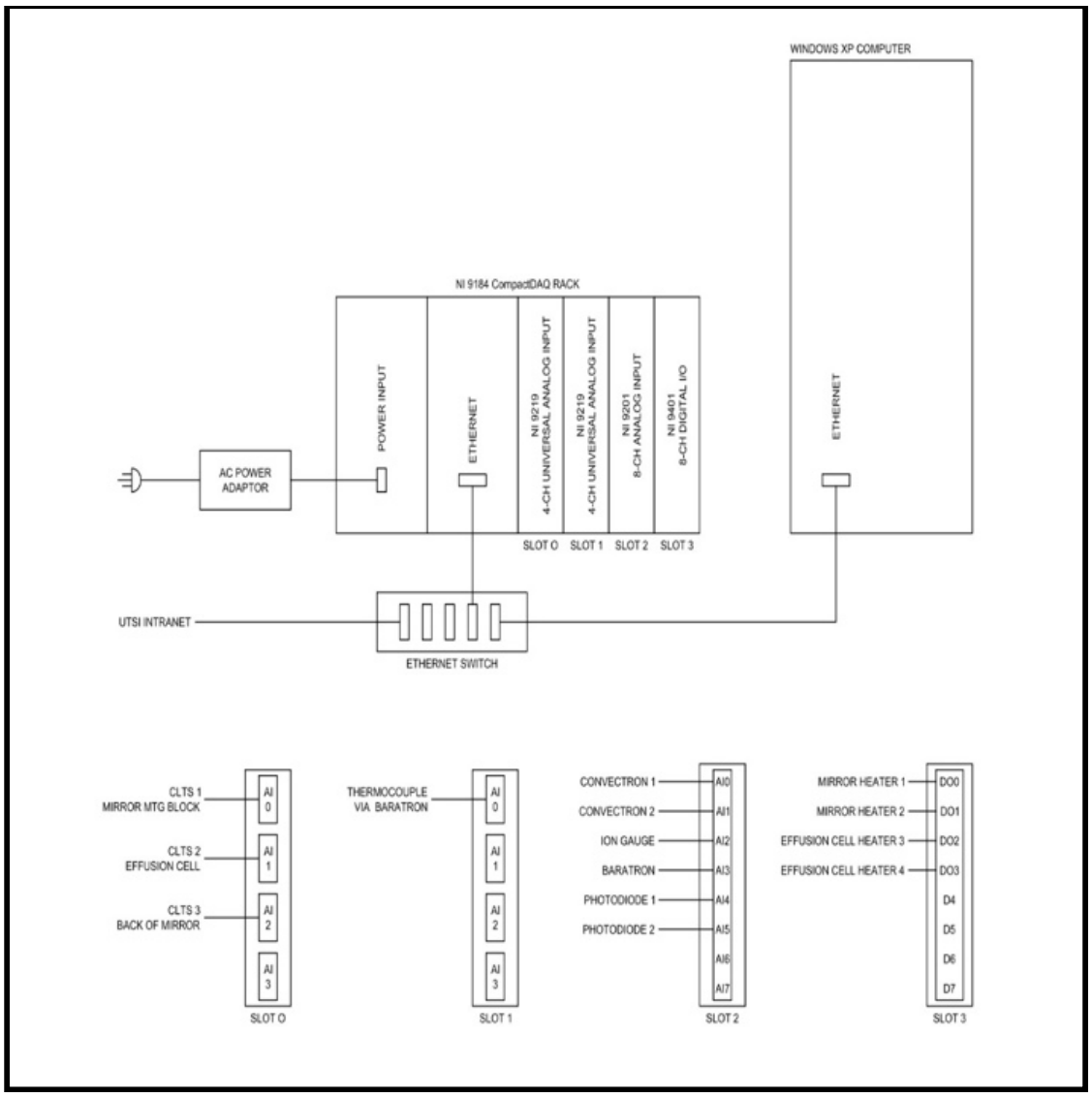

Figure 3.2. Data Acquisition Setup Schematic

The hydrated zeolite sample was inserted into a sample canister (refer to Figure 2.7 in the test setup section) and pumped down to approximately 0.1 Torr using a secondary roughing pump (see Figure 3.3).

A valve, initially isolating the sample chamber from the main chamber (Figure 3.4), was opened to allow the water vapor to flow to the effusion cell (refer to Figure 2.3).

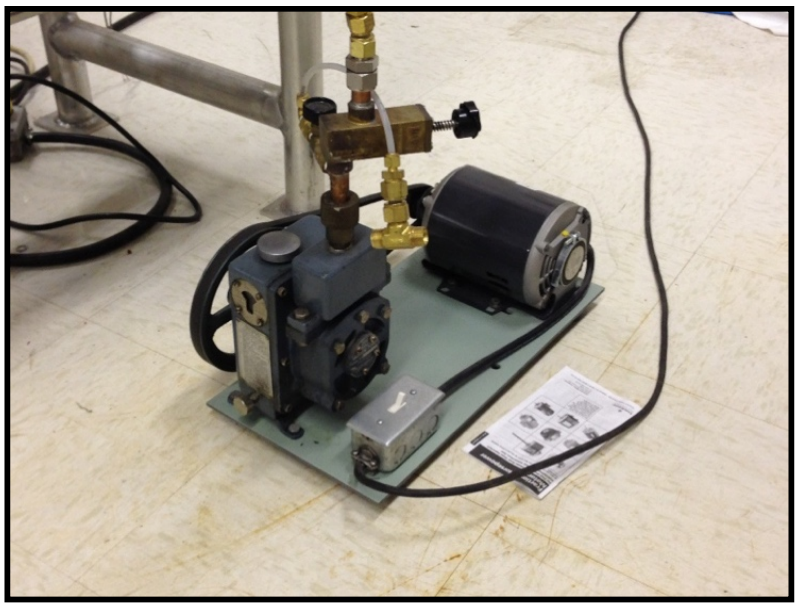

Figure 3.3. Secondary Roughing Pump.

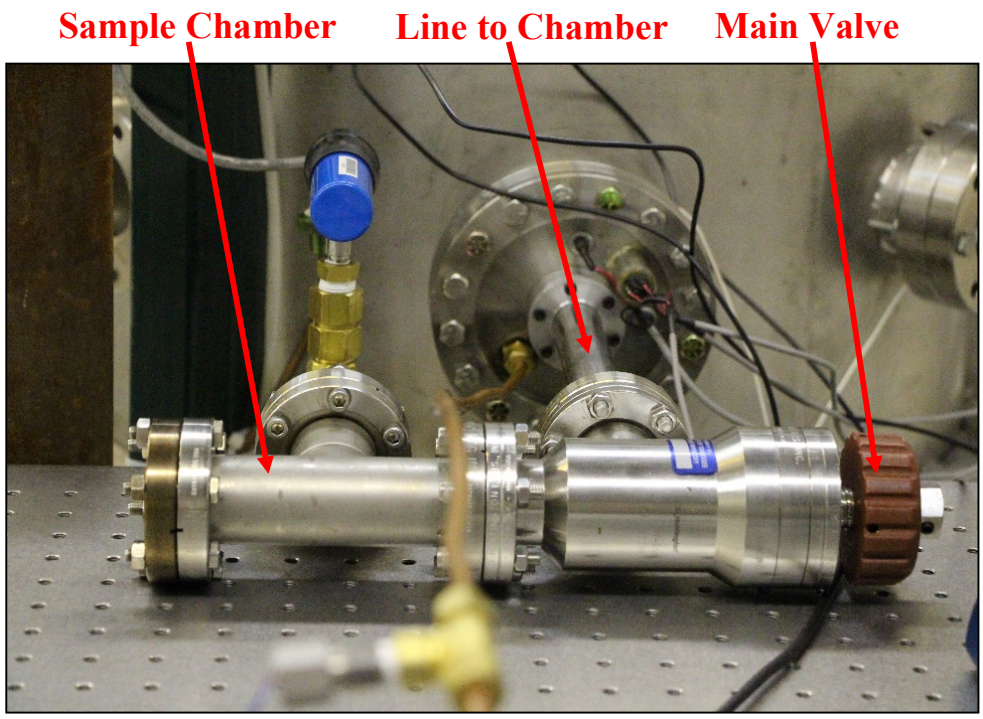

Figure 3.4. Sample Chamber, Main Valve, and Line to Main Chamber.

The 450 nm laser was turned on (Figures 3.5), and the stepper motor-controlled shutter (Figure 3.6) was then opened to allow the vapor to escape from the effusion cell and collect on the gold-plated mirror and QCM (See Figure 3.7). The shutter remained open for a minimum of one hour to permit adequate ice accumulation on the mirror and QCM surfaces.

Once the data were collected, the sample chamber was once again isolated from the main chamber by closing the main valve and the sample removed. The zeolite sample mass was then measured and compared to the pre-test mass to determine the total amount of water lost from the zeolite.

3.2 Baseline Test

A baseline test was performed to determine the behavior of the chamber in the absence of a hydrated zeolite sample. The procedure, as given in the previous section, was followed identically. A summary of the baseline test data is given in Table 3.1, where P_i and P_f are the initial and final chamber pressures, $T_{c,i}$ and $T_{c,f}$ are the initial and final chamber temperatures, and $T_{m,i}$ and $T_{m,f}$ are the initial and final temperatures of the cryo-cooled mirror mount.

Table 3.1. Baseline Test Data

Test Duration	P_i (Torr)	P_f (Torr)	$T_{c,i}$ (Kelvin)	$T_{c,f}$ (Kelvin)	$T_{m,i}$ (Kelvin)	$T_{m,f}$ (Kelvin)
5hr 14min	2.04×10^{-7}	4.78×10^{-7}	281.49	282.4	33.29	48.92

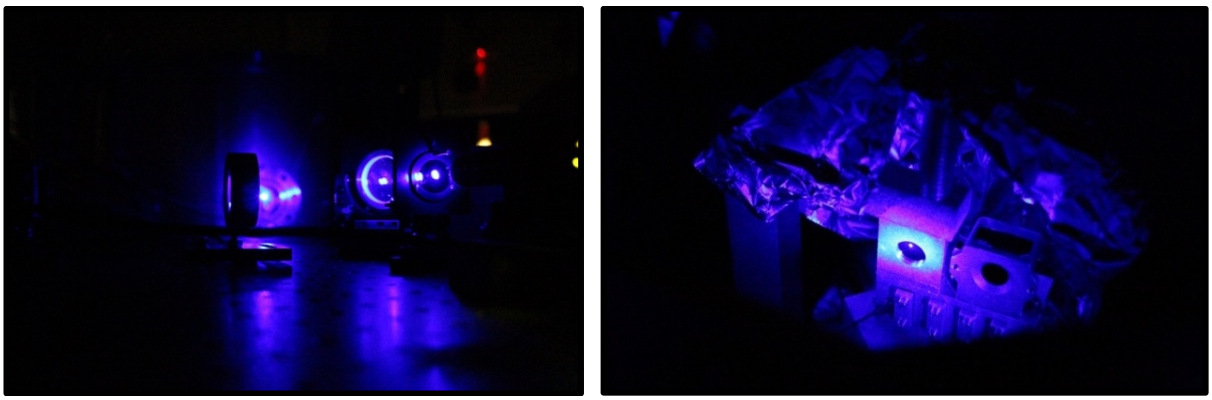

Figure 3.5. 450nm Laser Passing into Main Chamber (Left). Laser Beam Reflecting Off Mirror (Right).

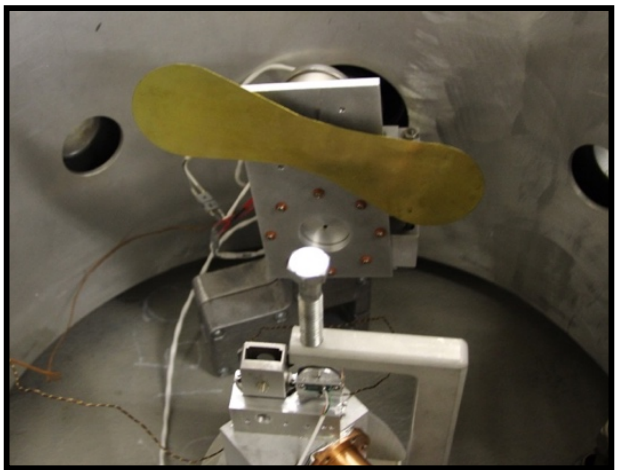

Figure 3.6. Shutter System

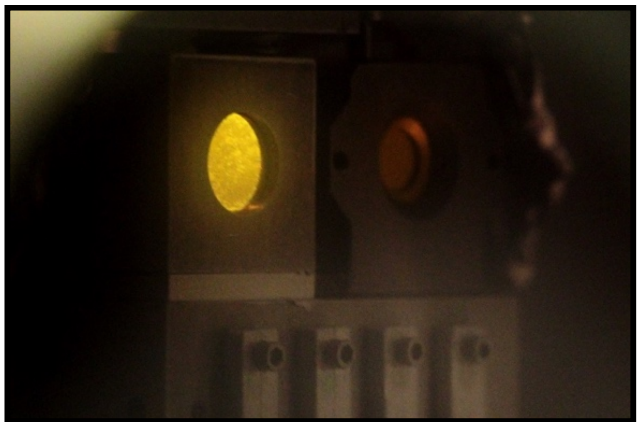

Figure 3.7. Gold-Plated Mirror and QCM with Ice Accumulation

3.3 Zeolite Preparation and Hydration

The zeolite sieves were baked out in a vacuum oven at a temperature of 423.2 K (150°C) for approximately twenty-four hours. Once the bake-out was complete, the sieves were separated into individual glass test canisters (Figure 3.9) and hydrated with DI (deionized) water using a dropper. The masses of the samples were then measured, the results of which are summarized in Table 3.2.

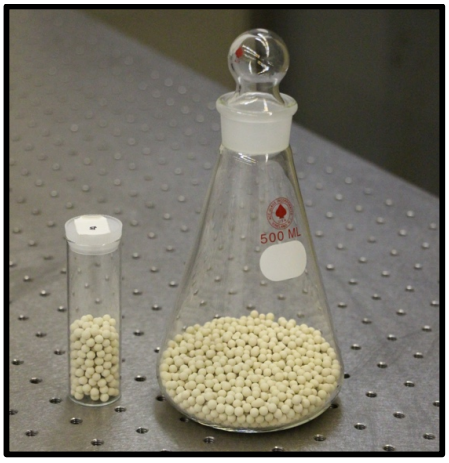

Figure 3.8. Zeolite Sieve Sample after Hydration

Table 3.2. Zeolite Sample Data

	Sample B	Sample C	Sample E
Date	**10-17-13**	**10-24-13**	**11-26-13**
Canister Mass	28.59	28.61	28.60
Zeolite Mass (g) (pre-hydration)	15.59	15.04	14.21
Zeolite Mass (g) (post-hydration)	17.51	17.07	16.08
Water Mass (g)	1.92	2.03	1.87

CHAPTER FOUR
ANALYSIS AND RESULTS

The interferometer and QCM data were analyzed using two C programs, as well as Microsoft Excel for basic plotting.

4.1 Optical Data Analysis

The program *opt_anal (optical analysis)* [17] was used to analyze the optical data. The program took into account that the incoming laser beam is polarized perpendicular to the plane of incidence, i.e., the plane containing the incident and reflected beams. The program required the following input: the ratios of the reflected beam to the incident beam (PD2/PD1), as well as the test start and end times. This information allowed the program to determine the length of the period of oscillation. As a visual example, refer to Figure 4.1, which shows the fringes recorded during a test. The start and end times are denoted on the image: all data points before and after these times are disregarded as they are simply noise values when the photodetectors were turned off.

4.2 QCM Analysis

QCM data analysis was performed by the program *qcm_anal (qcm analysis)* [18]. The purpose of this program was to determine how the ice thickness changes over time: the output is given in meters. The program first determined the resonant frequency of the crystal before any ice accumulated on the surface. This was accomplished by taking the first few seconds of data of the test before the shutter was open and averaging the values together. Refer to Figure 4.2 for a

visualization of this process: the start time and the values selected for averaging to determine the resonant frequency have been labeled on the image.

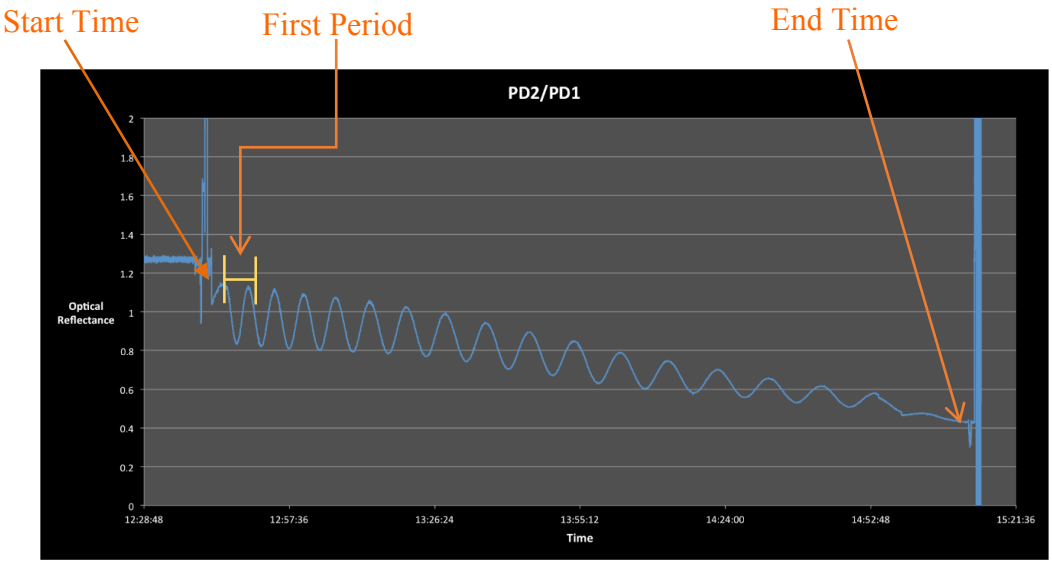

Figure 4.1. Example Input Data for Optical Analysis

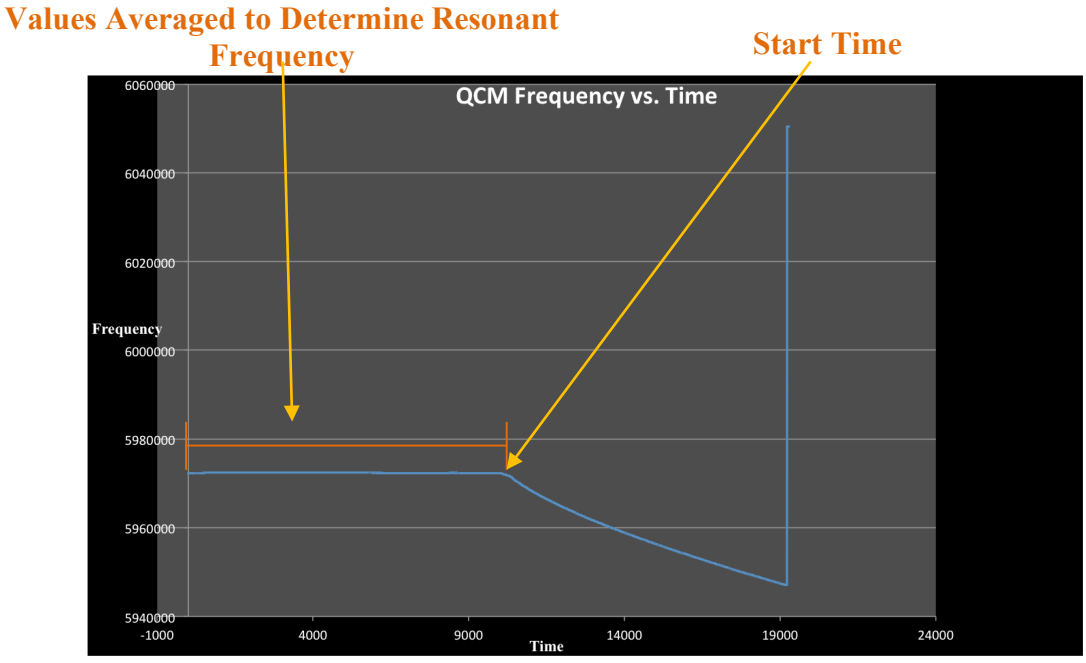

Figure 4.2. Example Input Data for QCM Analysis

4.3 Results of Zeolite Tests

Three experimental runs were performed after the initial baseline tests were completed. The first of these tests was performed on October 17th, 2013. At this time, the QCM was not yet operational, therefore the only data that could be collected was from the interferometer. The initial conditions for this test are summarized in Table 4.1

Table 4.1. 10-17-13 Test Conditions

P_i (Torr)	2.88×10^{-6}
$T_{c,i}$ (Kelvin)	288.37
$T_{m,i}$ (Kelvin)	31.08

After allowing the chamber to pump down and cool for nearly a day, the test procedure in Section 3.1 was implemented. Once the sample chamber was opened and water vapor from the zeolite sieves was released into the chamber, data was taken for two hours and six minutes. Figure 4.3 shows the ratio of the two photodiodes over time. The photodiode ratio became smaller and smaller as time progressed due to ice accumulation on the mirror. Note that the sudden dip in the photodiode ratio at the approximate 18:21:00 time mark (Figure 4.3) was due to an incident where the beam was inadvertently blocked as it exited the chamber for a moment while equipment was being checked.

Initially, the hydrated zeolite sample used for this test had a mass of 17.53 grams. After testing was completed, the total mass of the zeolite had been reduced to 17.46 grams, thus indicating that a mass of 0.07 grams of water had been transferred into the chamber when the

sample chamber was opened. The ice thickness values on the mirror surface over time is shown in Figure 4.4. In roughly 1.5 hours, 3 microns of ice had grown on the surface of the gold mirror.

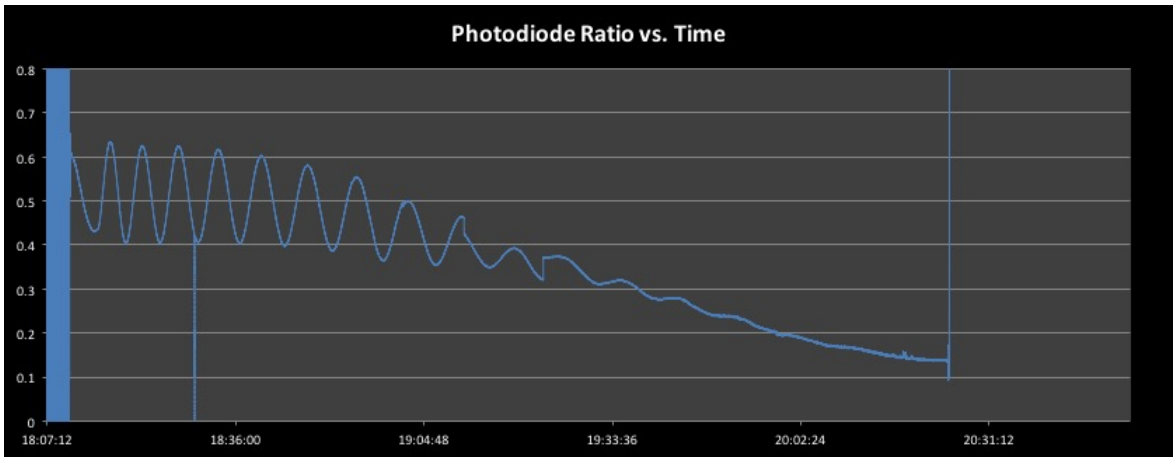

Figure 4.3. 10-17-13 PD vs Time

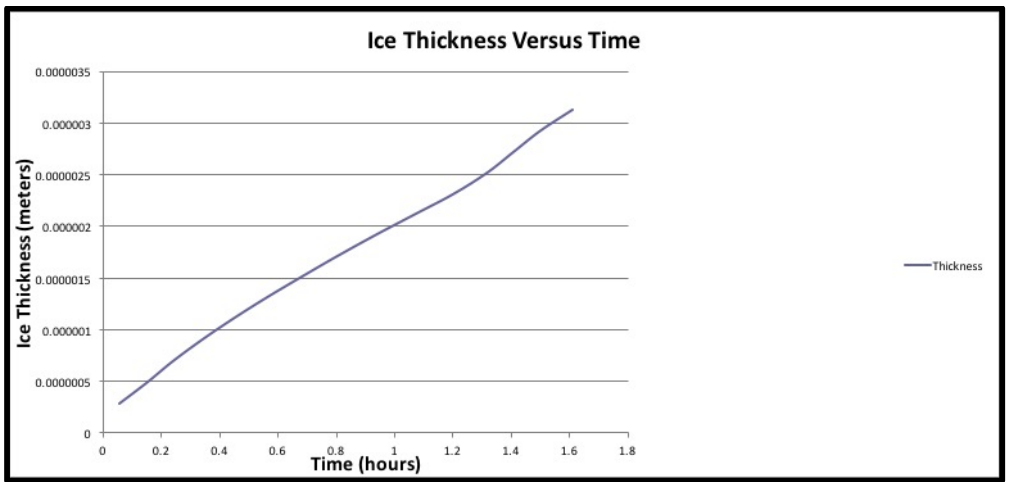

Figure 4.4. 10-17-13 Ice Thickness (Mirror Only, No QCM)

The second run on October 24th, 2013 introduced its own set of unique issues. On October 18th, a leak was detected around the flange of the copper tube that ran from one of the

baratron pressures gauges into the main chamber (see Figure 4.6). A high-vacuum epoxy sealant was used to plug the leak so a minimum initial pressure of 10^{-6} Torr could be reached.

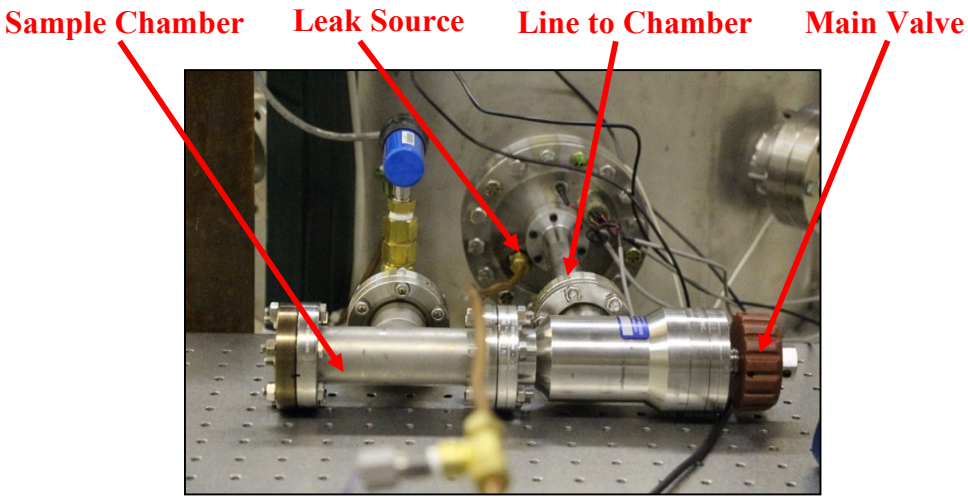

Figure 4.5. Leak Source.

Once the leak was plugged, the chamber was cooled and pumped down to achieve acceptable testing conditions. For this run, both the interferometer and QCM were operational, allowing us to measure ice accumulation on both the gold-plated mirror and quartz crystal surfaces. The initial conditions for this run are outlined in Table 4.2.

Table 4.2. 10-24-13 Test Conditions

P_i (Torr)	9.5×10^{-8}
$T_{c,i}$ (Kelvin)	288.07
$T_{m,I}$ (Kelvin)	32.72

We again saw the same trend with the photodiode ratio and mirror reflectance plots. As time progressed through the run, the photodiode ratio and mirror reflectance fell as ice accumulated onto the mirror surface (see Figure 4.6).

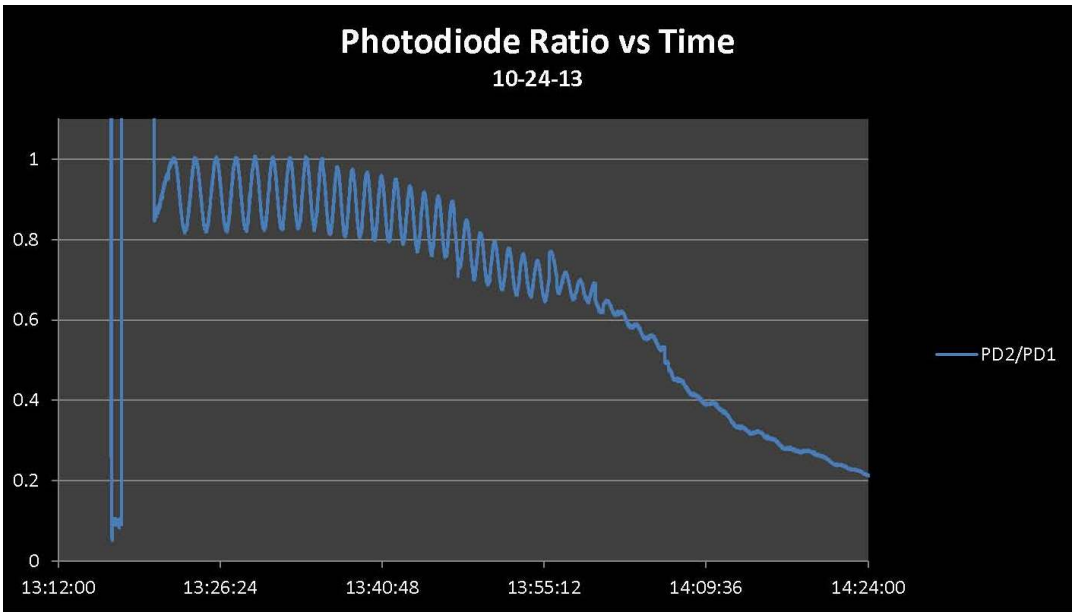

Figure 4.6. 10-24-13 PD Ratio vs Time.

Initially, the hydrated zeolite sample used for this test had a mass of 17.05 grams. After testing was completed, the total mass of the zeolite had been reduced to 16.54 grams, thus indicating that a mass of 0.51 grams of water had been transferred into the main chamber when the sample chamber was opened. Over the course of the two-hour and thirty-two-minute test, steady ice growth was detected on both the gold-plated mirror and the QCM surfaces. At the end of the test, the interferometer measured the ice accumulation to be approximately 6.06 microns, while the QCM had a measured ice growth of 4.61 microns. This gave a percent difference of ice growth measurement between the two instruments of 27.1%. A comparison of the interferometer and QCM ice thickness measurements can be seen in Figure 4.7.

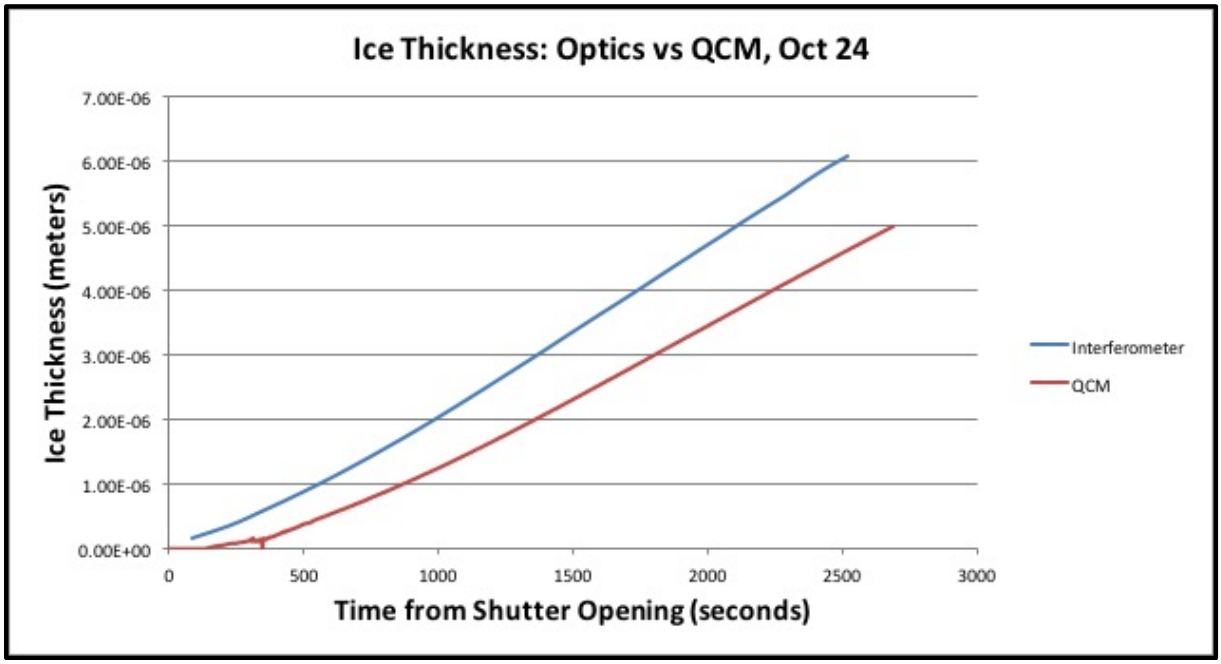

Figure 4.7. 10-24-13 Ice Thickness (Mirror and QCM).

The final run was performed on November 26th, 2013. The initial testing conditions for this run are summarized in Table 4.3. During this run, the lowest initial testing temperature recorded on the mirror mount was achieved.

Table 4.3. 11-26-13 Test Conditions

P_i (Torr)	2.44×10^{-6}
$T_{c,i}$ (Kelvin)	282.19
$T_{m,I}$ (Kelvin)	29.83

Neglecting the noise seen at the beginning and end of the test results, the same trend of decreasing photodiode ratio over time was again observed during the phase of ice accumulation (See Figure 4.8).

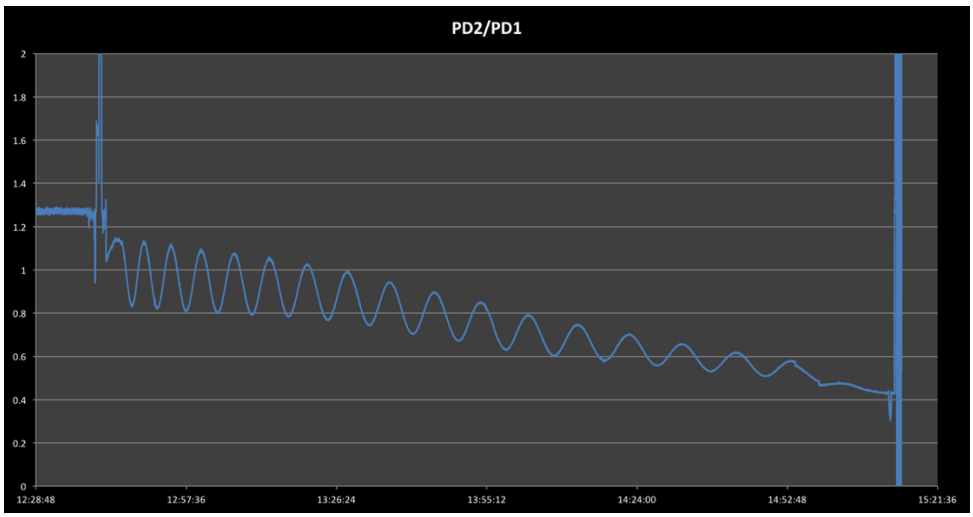

Figure 4.8. 11-26-13 PD Ratio vs Time

Initially, the hydrated zeolite sample used for this test had a mass of 16.04 grams. After testing was completed, the total mass of the zeolite had been reduced to 15.9 grams, thus indicating that a mass of 0.14 grams of water had been transferred into the main chamber when the sample chamber was opened. Over the course of the two-hour and thirty-two-minute test, steady ice growth was detected on both the gold-plated mirror and the QCM surfaces. At the end of the test, the interferometer measured the ice accumulation to be approximately 3.25 microns, while the QCM had a measured ice growth of 2.88 microns. This gave a percent difference of ice growth measurement between the two instruments of 12.2%, a much better number than was found in the second run. A comparison of the interferometer and QCM ice thickness measurements is given by the plot in Figure 4.9, while a summary of the conditions and results from all three data runs can be found in Table 4.4

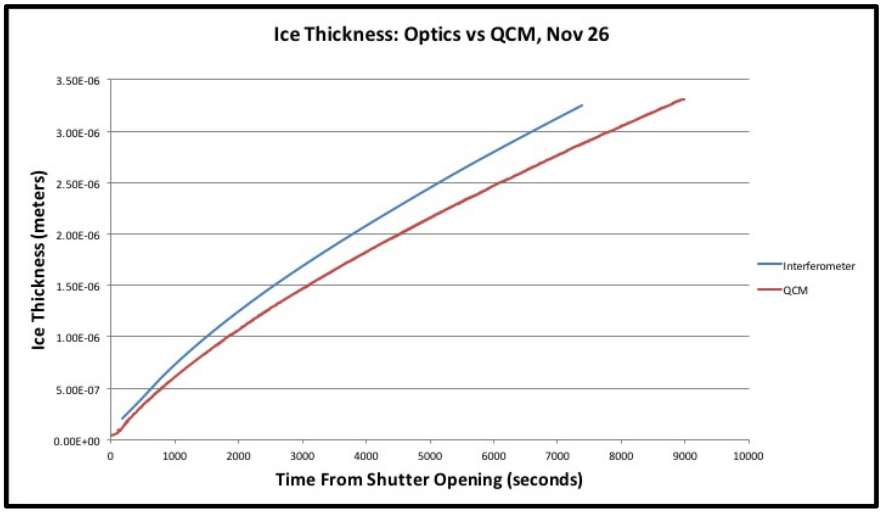

Figure 4.9. 11-26-13 Ice Thickness (Mirror and QCM).

Table 4.4. Zeolite Test Data

Date	Sample B	Sample C	Sample E
Sample	**10-17-13**	**10-24-13**	**11-26-13**
Test Duration	2hr 06min	2hr 32min	2hr 32min
P_i (Torr)	2.88×10^{-6}	9.5×10^{-8}	2.44×10^{-6}
P_f (Torr)	1.95×10^{-6}	2.02×10^{-6}	1.26×10^{-5}
$T_{c,i}$ (K)	288.37	288.07	282.19
$T_{c,f}$ (K)	288.36	287.68	281.77
$T_{m,i}$ (K)	31.08	32.72	29.83
$T_{m,f}$ (K)	31.59	77.60	39.46
Zeolite Mass (g) (pre-test)	17.53	17.05	16.04
Zeolite Mass (g) (post-test)	17.46	16.54	15.90
Water Mass (g)	1.92	2.03	1.87
Total Mass Loss (g)	0.07	0.51	0.14
Interferometer Ice Thickness (μm)	N/A	6.06	3.25
QCM Ice Thickness (μm)	N/A	4.61	2.88
Percent Difference (Ice Thicknesses)	N/A	27.1%	12.2%

CHAPTER FIVE
CONCLUSIONS AND FUTURE WORK

5.1 Conclusions

The zeolite tests performed in the SAM chamber were successful in that they provided sound evidence that the concept of tracking ice growth using an interferometer and QCM system would, indeed, accomplish the task. Once the QCM was operational and working in conjunction with the interferometer, the data obtained with both instruments tracked each other quite well. All three test runs showed steady ice growth, which could be seen by the decrease in the photodiode ratio over the duration of the experiments (refer to Figures 4.3, 4.7, and 4.10).

The test performed on October 24th showed that the interferometer and QCM systems were detecting ice growth on both the gold-plated mirror and crystal surfaces. The resulting 27.1% difference between the ice thickness measurements of the interferometer and QCM were, at first glance, disconcerting. After completion of the experiment, the reason for such a high percent difference in measurements was discovered. Six days prior to this test, a leak was discovered around brass hardware on the flange connecting to the effusion cell. Due to the design of the fitting on the hardware, it was impossible to tighten down the nut without allowing more air to enter the chamber. The only solution, given the available time and budget, was to completely rebuild the flange and change the hardware which, unfortunately, was not option during this phase of the project. A temporary solution to the problem was to attempt to seal the leak using a high-vacuum epoxy sealant. This sealant, while it did fix the leak, became a contamination source while the epoxy hardened. Particles from the epoxy were pulled into the

chamber and formed a thin layer on both the gold-plated mirror and QCM surfaces. Our interferometer data analysis program, while it did account for the index of refraction for ice on the mirror surface, obviously did not take into account the index of refraction for the epoxy sealant. While the QCM was also affected by this contamination, the method in which the ice thickness was calculated (using the mass to determine the shift in frequency of the crystal) averaged out the mass that was already on the QCM just before the test began (refer to Figure 4.11 and how the QCM measurements start at zero). This discrepancy in the interferometer data caused a higher-than-normal percent difference between the two instruments. Once this contaminant was identified, the gold-plated mirror was cleaned and a new crystal was placed in the QCM.

The cause for discrepancies between the interferometer and QCM ice growth measurements was not limited to contamination factors on our instrument surfaces. One likely source of error was the alignment of the mirror mount with the opening of the effusion cell. Due to the mounting system used (the C-clamp keeping the mirror and QCM mount secured to the aluminum block) and the location of the mount within the chamber, it was impossible to ensure the effusion cell opening was perfectly centered between the gold-plated mirror and the QCM. If the opening was not properly centered, this could have caused more water to deposit on one test surface than the other, thus causing more ice to form on that particular test surface than its counterpart. In addition, if the mirror mount was not aligned parallel to the effusion cell causing either the mirror or the QCM to be rotated slightly away from the effusion cell opening, this would further exacerbate the issue of unequal water distribution of the test article surfaces.

After addressing the above-mentioned sources of error, the final test run performed on November 17th, 2013 gave the most promising results. With only a 12.2% difference in ice growth measurements between the QCM and interferometer, we saw that our method of obtaining accurate measurements with our system was a success. Future modifications to the SAM chamber setup will ensure a much higher accuracy in detecting ice thicknesses.

5.2 Future Work

As far as the data analysis is concerned, there is one possible modification that can be made to further improve the ice growth calculations as measured by the QCM. As discussed in Section 1.4, the mass of accumulated ice on the QCM surface is calculated by measuring the change in the frequency of the crystal. It has been suggested that if the temperature of the QCM crystal is not accurately measured, then the overall mass calculations will have additional uncertainty, meaning that the measured frequencies and, consequently, the accumulated ice mass calculations will have a larger margin of error [4]. It has been shown that when the following temperature correction is applied (see Equation 9), a much more accurate crystal frequency measurement is found [4].

$$\boldsymbol{F_{corr} = F_{measured} + \Delta F} \quad (9)$$

where F_{corr} is the corrected frequency (measured in Hz), $F_{measured}$ is the measured frequency, and ΔF is the frequency correction. Equation 10 shows the formula for calculating the frequency correction at a specific temperature, $T(K)$.

$$\boldsymbol{\Delta F = -49.34615385\, x\, T(K)} \quad (10)$$

When the temperature corrections, as shown in Equations 9 and 10 were applied and compared to the ice accumulation thicknesses measured by an interferometer, the values were much closer when an ice density value of 0.88 gm/cm^3 was used. It should be noted that when an ice density value of 0.94 gm/cm^3 was used in the ice thickness calculations instead of 0.88 gm/cm^3, as in the study by William Stevens [19], the interferometer and QCM ice thickness values achieved were within, on average, 2.8-7.4% of each other.

Several modifications can be made to the chamber itself, as well as to the testing procedure to yield longer test periods and an overall more precise method of data collection and analysis.

First, a relatively small portion of the total amount of water from the zeolite, compared to the amount the sieves contain, is actually released during the test period. Future tests should utilize an external heater to help more water to be released from the zeolite (see Figure 5.1).

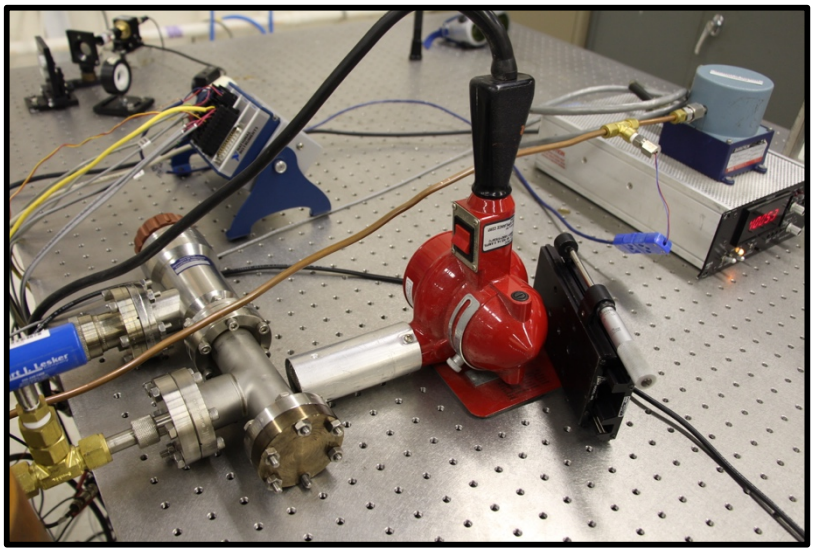

Figure 5.1. External Heat Source Applied to Sample Chamber.

Second, the mirror mount should be redesigned so that slight adjustments can be made without compromising the position of the entire mount, thus having to start the alignment process over from the beginning. The key to this is to eliminate the use of the C-clamp to hold the mount in place (see Figure 5.2): permanently attaching the mirror mount to the aluminum block and adding rotational adjusters to help with the laser/interferometer alignment would be an invaluable improvement.

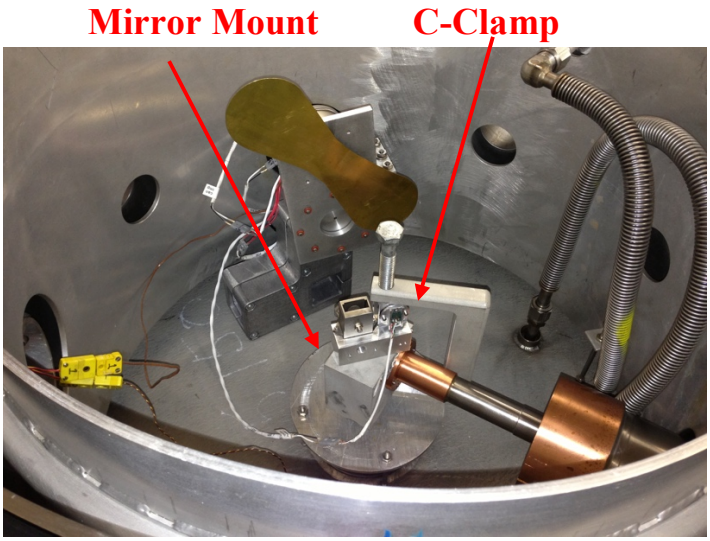

Figure 5.2. Mirror Mount and C-Clamp.

Third, a critical component that needs to be reevaluated is the effusion cell. While the data taken from the interferometer and QCM tracked each other fairly well, there were still unacceptably large margins of error in the measured ice accumulation values. Designing a system to ensure the gold-plated mirror and QCM surface are accumulating the same amount of water from the effusion cell is essential. With a consistently and properly aligned effusion cell, the likelihood of water being distributed on both of the test surfaces evenly will be much higher, thus eliminating such large discrepancies in the measured data.

Fourth, the two sources of leaks (the virtual leak on the valve connecting the sample chamber to the effusion cell and the leak around the flange housing the pipe running to the effusion cell) must be fixed. Eliminating the two leak sources will allow less air contamination in the chamber, will reduce pump-down time for the external sample chamber, and will help keep the pressure in the main chamber more constant while introducing a sample into the chamber.

The leak around the flange housing the pipe running to the effusion cell (Figure 5.3) was the cause of a significant amount of contamination during our initial tests. It was found that, due to the location of the brass hardware around the pipe, it was impossible to get a wrench secured around the nut to sufficiently tighten it down (see Figure 5.3). Because this piece of hardware was not able to be tightened enough to prevent a leak, it was suggested that we try to fix the leak by putting an epoxy coating around the flange to seal the system and prevent further leaks (see Figure 5.4).

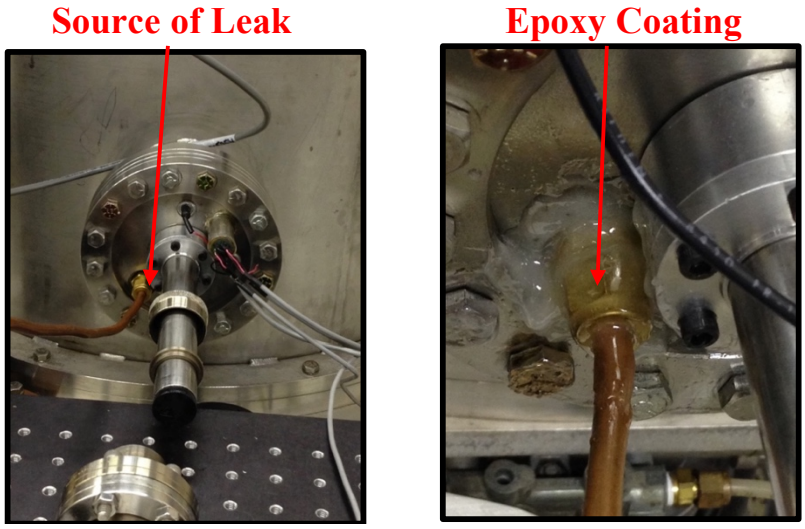

Figure 5.3. Leak Around Flange to Effusion Cell (Left) and Vacuum Sealant Around Flange (Right).

While this method was successful in sealing the chamber, it was catastrophic for our gold-plated mirror and QCM inside the chamber. Once the October 24th test began and the chamber began to pump down, particles from the epoxy were pulled into the chamber and covered the mirror and QCM surfaces. Fortunately, a solvent and microfiber cloth were sufficient enough to clean and salvage the mirror surface. Figures 5.4 and 5.5 show the non-contaminated mirror and QCM surfaces before the test, the contaminated mirror surface after the test, and the post-cleaning mirror surface, respectively. A new flange system will need to be installed to eliminate this component in order to ensure a proper seal and to protect the integrity of the mirror and QCM surfaces.

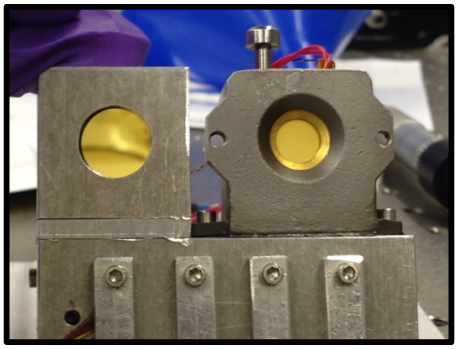

Figure 5.4. Uncontaminated Mirror (Left) and QCM Surface (Right).

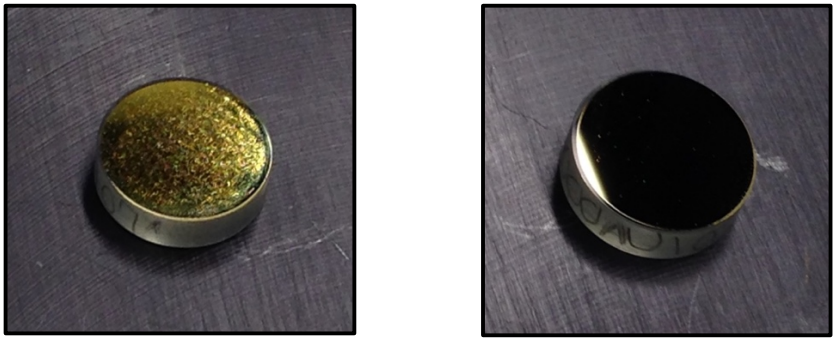

Figure 5.5. Contaminated Mirror (Left) and Decontaminated Mirror Surface (Right).

Finally, a new chamber for the zeolite samples should be designed. The current design, while functional, certainly has its drawbacks. After the five bolts on the flange are removed, you must break the seal on the sample chamber by brute force, thus creating the potential for a serious leak in the flange housing the effusion cell feedthrough or causing damage to the rubber gasket. Also, there is no way to easily remove the sample without using a tool to insert into the chamber, thereby risking contaminating not only your sample, but the chamber as well. In total, this process takes a minimum of 2-3 minutes, allowing additional contaminants to enter the sample chamber and jeopardizing the integrity of the final mass readings.

The goal for this project was to build a vacuum system that has the ability to detect the growth of thin films on cryo surfaces in high-vacuum environments. Eventually, there will be a need not only to grow thin films of ice on optical surfaces, but also to find a way to either a) eliminate the thin ice films without introducing additional heat into the system (thus interfering with optical readings and other instrumentation) or b) prevent the films from accumulating on the optical surfaces.

LIST OF REFERENCES

1. “An Introduction to Molecular Sieves,” http://www.eltrex.pl/pdf/karty/adsorbenty/ENG-Introduction%20to%20Zeolite%20Molecular%20Sieves.pdf.

2. Bertrand, W. A., *Solar Absorptance of Optical Surfaces Contaminated with Spacecraft Material Outgassing Products.* Final Report, Arnold Engineering and Development Complex, 1993.

3. Breck, D., *Zeolite Molecular Sieves: Structure, Chemistry, and Use.* John Wiley & Sons, Inc., 1974.

4. Collins, F., Analysis of QCM Measurements and Comparison with Interferometric Measurements.

5. Finckenor, M. M., A Researcher’s Guide to: Space Environmental Effects. Retrieved from https://www.nasa.gov/sites/default/files/files/NP-2015-03-015 JSC_Space_Environment-ISS-Mini-Book-2015-508.pdf, 2015.

6. Heavens, O.S., “Optical Properties of Thin Solid Films,” Dover, New York, 1991.

7. Kiefert, N. “New Interactive Chart Shows Just How Many Satellites Are Orbiting Earth.” Retrieved from http://www.astronomy.com/news/2017/01/interactive-satellite-chart, 2017.

8. Liu, C.K., “Degradation of Cold Optical Systems by Cryodeposition, Report for 1971 Independent Research Program,” *AD – 756772,* Lockheed Missiles and Space Company, Palo Alto, California, February, 1972.

9. Llano-Restrepo, M. A., “Accurate Correlation, Thermochemistry, and Structural Interpretation of Equilibrium Adsorption Isotherms of Water Vapor in Zeolite 3A by Means of a Generalized Statistical Thermodynamic Adsorption Model,” *Fluid Phase Equilibria, 283*, 73-88, 2009.

10. Lu, C.S. and Lewis, O., “Investigation of film-thickness determination by oscillating quartz resonators with large mass load,” J.Appl. Phys.43(11), 4385, JAPIAU0021-8979, 1972.

11. Moeller, T. S., “Measurement of the Accumulation of Water Ice on Optical Components in Cryogenic Vacuum Environments,” *Optical System Contamination: Effects, Measurements, and Control, 8492*, 2012.

12. O'Hanlon, J., *A User's Guide to Vacuum Technology.* Hoboken, New Jersey, John Wiley and Sons, Inc., 2003

13. Rogers, J., “Introducting Water Vapor Into a High Vacuum Chamber at AEDC,” 2011.

14. Sauerbrey, G., “Use of crystal oscillators for weighing thin films and for microweighing,” Zeitschrift fuer Physik155(2), 206–222, 1959.
15. Smith, A. “The Quartz Crystal Microbalance,” in *Handbook of Thermal Analysis and Calorimetry*, Vol. 5, Elsevier, Amsterdam, 2008.

16. Smith, L. M., *PSI Report #1*, 2013.

17. Smith, L. M., Opt_Anal.cpp (C++ Source Code), University of Tennessee Space Institute, Tullahoma, TN, October 2013.

18. Smith, L. M., QCM_Anal.c (C++ Source Code), University of Tennessee Space Institute, Tullahoma, TN, October 2013.

19. Stevens, W.A., “Measurement of Water Ice Accumulation on a First Surface Gold Mirror Under Cryogenic, High-Vacuum Conditions,” UT Master’s Thesis, 2016.

20. Westley, Michael Scott. “Vapor Deposited Water Ice: Structural Properties, Effects of Ultraviolet Light, and Astrophysical Implications.” Master’s Thesis. University of Virginia, 1994.

21. Westley, Michael Scott., “Density and Index of Refraction of Water Ice Films Vapor Deposited at Low Temperatures,” *Journal of Chemical Physics*, February 1998.

22. Yang, R., *Adsorbents: Fundamentals and Applications.* John Wiley & Sons, Inc., 2003.

23. “Zeolite,In *Encyclopedia Britannica.* Encyclopedia Britannica, Inc., 2002.

VITA

Sabrina Hurlock was born in Kingsport, TN, to the parents of Linda Brown and Rickey Hurlock, and has one sister, Amber Hurlock. Upon graduation from Sullivan North High School in Kingsport, she attended East Tennessee State University where she earned her Honors-In-Discipline B.S. degree in physics, with a thesis entitled "Automated Detection of Coronal Mass Ejections Using Advanced Coronal Image Separation Methods" in 2010. In 2012, she accepted a graduated research assistantship at the University of Tennessee Space Institute to pursue a Master of Science degree in Engineering Science with a concentration in Mechanical Engineering, specifically Thermal Fluids/Fluid Mechanics. She is currently teaching chemistry and physics at LaVergne High School.